



Determination of the substorm initiation region from a major conjunction interval of THEMIS satellites

A. Lui, V. Angelopoulos, O. Lecontel, H. Frey, E. Donovan, D. Sibeck, W. Liu, H. Auster, D. Larson, Xiaojian Li, et al.

► To cite this version:

A. Lui, V. Angelopoulos, O. Lecontel, H. Frey, E. Donovan, et al.. Determination of the substorm initiation region from a major conjunction interval of THEMIS satellites. *Journal of Geophysical Research Space Physics*, 2008, 113 (A1), pp.A00C04. 10.1029/2008JA013424 . hal-03086700

HAL Id: hal-03086700

<https://hal.science/hal-03086700>

Submitted on 29 Jan 2021

HAL is a multi-disciplinary open access archive for the deposit and dissemination of scientific research documents, whether they are published or not. The documents may come from teaching and research institutions in France or abroad, or from public or private research centers.

L'archive ouverte pluridisciplinaire **HAL**, est destinée au dépôt et à la diffusion de documents scientifiques de niveau recherche, publiés ou non, émanant des établissements d'enseignement et de recherche français ou étrangers, des laboratoires publics ou privés.

Determination of the substorm initiation region from a major conjunction interval of THEMIS satellites

A. T. Y. Lui,¹ V. Angelopoulos,² O. LeContel,³ H. Frey,⁴ E. Donovan,⁵ D. G. Sibeck,⁶ W. Liu,⁷ H. U. Auster,⁸ D. Larson,⁴ X. Li,⁷ M. Nosé,⁹ and M. O. Fillingim⁴

Received 23 May 2008; revised 22 July 2008; accepted 5 September 2008; published 5 December 2008.

[1] We investigate in detail the time history of substorm disturbances in the magnetotail observed during a major tail conjunction of Time History of Events and Macroscale Interactions during Substorms (THEMIS) satellites on 29 January 2008, 0700–0900 UT. During this interval, all THEMIS satellites were closely aligned along the tail axis near midnight and were bracketed in local time by GOES 11 and 12. The radial distance covered ranges from the geosynchronous altitude to $\sim 30 R_E$ in the tail. This interval consists of three activations detected by the THEMIS satellites with good ground all-sky-camera observations of auroral activity. The first activation is a small substorm with spatially limited disturbance in the tail. The onset arc was equatorward of an undisturbed arc. The second activation is a moderate size substorm with the onset arc also being equatorward of an undisturbed arc. The third activation is an intensification of the substorm with its onset indicated by the second activation. The active auroral arc for this intensification was near the poleward boundary of the auroral oval. Analysis of these observations indicates that the first activation is a small substorm initiated in the near-Earth plasma sheet and does not involve magnetic reconnection of open magnetic field lines. Magnetic reconnection on closed field lines can be ruled out for this substorm because it cannot generate the observed high-speed plasma flow. The second and third activations are part of a moderate size substorm initiated also in the near-Earth plasma sheet, with a subsequent substorm intensification involving activity initiated tailward of $\sim 30 R_E$. Overall, the time history of substorm activity for these two substorms is consistent with the near-Earth initiation model.

Citation: Lui, A. T. Y., et al. (2008), Determination of the substorm initiation region from a major conjunction interval of THEMIS satellites, *J. Geophys. Res.*, 113, A00C04, doi:10.1029/2008JA013424.

1. Introduction

[2] Impulsive energy release events in space plasmas challenge our comprehension on how space plasmas can efficiently transform energy from one form to another. There are several impulsive energetic phenomena in the

plasma universe. Solar flares, coronal mass ejection, magnetospheric substorms, gamma-ray bursts, astrophysical jets are some well-known examples. Of all of these phenomena, the one that can be investigated with detailed in situ measurements is magnetospheric substorm. The concept of substorms was introduced through analysis of auroral morphology in the polar region from a network of all-sky-cameras [Akasofu, 1964]. It was subsequently expanded to encompass related disturbances throughout the magnetosphere.

[3] In the early era of substorm research, magnetic reconnection is regarded as the primary physical process for substorm expansion onset. The magnetic field configuration for magnetic reconnection is to be achieved by the tearing instability [Coppi *et al.*, 1966; Schindler, 1974]. However, the presence of a finite magnetic field normal to the neutral sheet in the magnetotail tends to suppress spontaneous onset of tearing instability by electron compressibility [Pellat *et al.*, 1991; Brittnacher *et al.*, 1998]. The tearing instability is stabilized because the energy required to compress the electrons from current filamentation created by the instability exceeds the available free energy from the magnetic field configuration. However, recent theoretical studies indicate that magnetic reconnection

¹Applied Physics Laboratory, Johns Hopkins University, Laurel, Maryland, USA.

²Institute of Geophysics and Planetary Physics, University of California, Los Angeles, California, USA.

³Centre d'Etude des Environnements Terrestre et Planétaires, Institut Pierre-Simon Laplace, Velizy, France.

⁴Space Sciences Laboratory, University of California, Berkeley, California, USA.

⁵Department of Physics and Astronomy, University of Calgary, Calgary, Alberta, Canada.

⁶NASA Goddard Space Flight Center, Greenbelt, Maryland, USA.

⁷Laboratory for Atmospheric and Space Physics, University of Colorado, Boulder, Colorado, USA.

⁸Institut für Geophysik und Extraterrestrische Physik, Technische Universität Braunschweig, Braunschweig, Germany.

⁹Department of Geophysics, Graduate School of Science, Kyoto University, Kyoto, Japan.

tion can be initiated with enhanced dissipation from the cross-field current instability [Lui *et al.*, 1991], or with the presence of transient electrons in the free energy budget [Sitnov *et al.*, 1997], or by departure of the current sheet from the Harris current sheet to gain additional free energy to drive the instability [Zelenyi *et al.*, 2008]. In spite of these possibilities, the viability of the tearing instability to create a magnetic reconnection site in the magnetotail is still an open question because the proposed current sheet features required to initiate tearing instability have not been verified observationally at the magnetic reconnection site in the magnetotail.

[4] There are other physical processes proposed for substorm onset that do not rely on magnetic reconnection, such as various forms of ballooning instability [Roux *et al.*, 1991; Voronkov *et al.*, 1997; Liu, 1997; Bhattacharjee *et al.*, 1998; Cheng and Lui, 1998; Pu *et al.*, 1999; Erickson *et al.*, 2000; Dobias *et al.*, 2004], cross-field current instability [Lui *et al.*, 1991], entropy anti-diffusion instability [Lee *et al.*, 1998], current-driven Alfvénic instability [Perraut *et al.*, 2000], convection reduction [Lyons *et al.*, 2003], and “akis” structure in a thin current sheet [Sarafopoulos, 2008].

[5] On the observational side, early indications that magnetic reconnection is the substorm onset process are reports of reversals in the B_z component at the neutral sheet [Nishida and Nagayama, 1973] and the occurrence of tailward plasma flows [Hones, 1973] during substorm expansions. These features form the basis of the near-Earth neutral line model for substorms. However, a reexamination of the reported B_z reversal events shows that they did not occur at the neutral sheet but at the high-latitude plasma sheet. The negative B_z component only constitutes a small percentage of the magnetic field magnitude, thus corresponding to only slight southward dipping of the magnetic field [Lui *et al.*, 1976]. A subsequent statistical study indicates that southward dipping is quite commonly observed associated with plasma sheet thinning in the magnetotail during substorm expansions [Lui *et al.*, 1977a]. Furthermore, the occurrence of tailward plasma flows during substorm expansions is rather infrequent [Lui *et al.*, 1977b].

[6] The latest version of the near-Earth neutral line model, also called the midtail initiation (MTI) model, invokes magnetic reconnection at downstream distances of 20–30 R_E [Nagai *et al.*, 1998]. The near-Earth substorm disturbances in this model are conveyed from midtail to the near-Earth region by means of bursty bulk flows (BBFs) recognized by Angelopoulos *et al.* [1992, 1994, 1997]. Dipolarization in the near-Earth region is caused by pileup of magnetic flux carried to the near-Earth region by earthward BBFs [Haerendel, 1992; Shiokawa *et al.*, 1997, 1998]. Most global MHD simulations of the magnetosphere reproduce this scenario [Lyon *et al.*, 1998; Raeder *et al.*, 2001]. Substorm onsets are associated with magnetic reconnection of open magnetic field lines because it is energetically favorable to account for explosive energetic phenomena and for high-speed plasma flows observed during substorms.

[7] Motivated by several observations that indicate near-Earth activity as the origin of substorm expansion disturbances, several substorm researchers proposed onsets to be in the near-Earth region [Lui, 1991, 1996; Erickson, 1995; Lyons, 1996; Lee *et al.*, 1998; Perraut *et al.*, 2003; Chen *et al.*, 2003; Saito *et al.*, 2008; Liang *et al.*, 2008; Donovan *et al.*, 2008].

In this near-Earth initiation (NEI) model, the onset process causes current disruption in the near-Earth region inside the downstream distance of $\sim 15 R_E$. Current disruption gives rise to non-MHD turbulence as demonstrated by Consolini *et al.* [2005]. The validity of the term turbulence to describe the large magnetic and electric fluctuations during current disruption is also demonstrated by the multiscale and multifractal nature of these disturbances [Lui, 2002]. As a result of current disruption, the magnetic field relaxes to a more dipolar configuration, giving rise to dipolarization and fast plasma flows [Lui *et al.*, 1993]. The current disruption process instigates further current disruption in adjacent locations by thinning the plasma sheet and enhancing the cross-tail current. This allows current disruption to occur progressively down the magnetotail. Later, magnetic reconnection may develop in one of these current disruption sites. This substorm model is also known as the substorm synthesis model since it combines current disruption process in the near-Earth with magnetic reconnection in the midtail region. It is consistent with results from riometer data to infer substorm injection location [Spanswick *et al.*, 2007] and the existence of two classes of BBFs [Shue *et al.*, 2008]. Some global MHD simulations reproduce the development of dipolarization in the near-Earth region being unconnected to midtail plasma flows intruding into that region [Tanaka, 2000; El-Alaoui, 2001].

[8] The past extensive substorm research thus leads to the existence of two substorm paradigms. It is imperative to determine which of these two scenarios is valid for further progress in substorm research. In a timely fashion, NASA's most recent magnetospheric mission THEMIS, an acronym for Time History of Events and Macroscale Interactions during Substorms [Angelopoulos, 2008], has the primary objective to resolve the controversy concerning the substorm initiation location in the magnetotail by placing five identically instrumented satellites aligned along the tail axis to determine incontrovertibly the propagation direction of substorm disturbances in the magnetotail.

[9] In this paper, we examine one major tail conjunction interval of THEMIS satellites when three substorm disturbances were observed by the inner probes of THEMIS D and E. The alignment of the THEMIS satellites along the tail direction is complemented with GOES 11 and 12 at two adjacent local times bounding that of the THEMIS satellites. In terms of time history, the NEI model predicts that the time sequence of earthward plasma flow to proceed from the near-Earth region to the midtail whereas the MTI model predicts the opposite time sequence. It is found that the first substorm activity is a localized activity with onsets of dipolarization, plasma flows, and particle energization developing progressively in the tailward direction starting from the near-Earth region. The second substorm activity has the same progressive development. On the other hand, the third substorm activity, which is a substorm intensification during ongoing substorm activity, has the opposite trend of disturbance development. Overall, the combined temporal sequence of the second and third substorm activities is consistent with the scenario proposed by the substorm synthesis model.

[10] The organization of the paper is as follows. Section 2 presents the ground-based observations to establish the

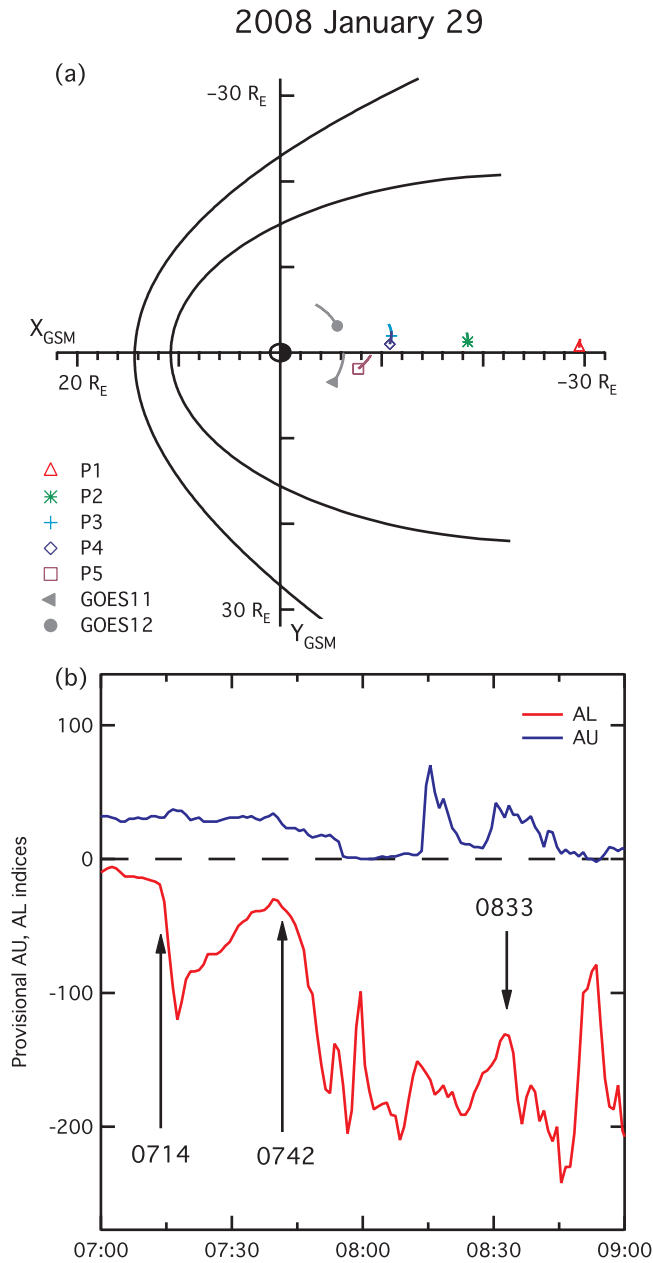


Figure 1. (a) The locations of the THEMIS satellites, GOES 11, and GOES12 projected on the GSM equatorial plane during the major tail conjunction interval on 29 January 2008. (b) The AU/AL indices during this interval, which consists of one isolated substorm started at ~ 0714 UT and a moderate size substorm with several intensifications.

reference times of substorm activity. The satellite observations are then presented in section 3. The time history of substorm development is ascertained in section 4, followed by summary and discussion in section 5.

2. Ground-Based Observations

2.1. Major Tail Conjunction Interval and Auroral Electrojet Indices

[11] The period of interest is a major tail conjunction of THEMIS on 29 January 2008, 0700–0900 UT when all five

satellites are lined up along the tail axis. The locations of the five THEMIS satellites and the two geosynchronous satellites GOES 11 and 12 during this interval are shown in Figure 1a in the GSM coordinates. The symbols denote the locations at the beginning of the interval, i.e., at 0700 UT on 29 January 2008, and their trajectories during the interval are indicated by the curve from their initial locations. All satellites were close to the midnight meridian. THEMIS A and GOES 11 were situated in the premidnight local times while the others were situated past the midnight meridian. The local times of the two GOES satellites bracket that of the five THEMIS satellites.

[12] The provisional AU/AL indices during this major conjunction are shown in Figure 1b, indicating the presence of substorm activity. The AL index started to decrease significantly from the quiet time level at ~ 0714 UT. The lowest AL index for this isolated substorm was only -120 nT at ~ 0717 UT and returned to a value close to the quiet time level of -30 nT at ~ 0739 UT. Thus, this is a small isolated substorm lasting for ~ 0.5 h. This activity was followed by another moderate size substorm. The AL index for this substorm started to show a significant decrease suggestive of substorm expansion onset at ~ 0742 UT. This activity was followed by a rather continuous electrojet activity till the end of the interval. Intermittent intensifications occurred at ~ 0754 , ~ 0800 , ~ 0813 , and ~ 0833 UT. Three instances of time particularly relevant to the auroral activations seen by the THEMIS all-sky-camera network and disturbances detected by THEMIS satellites are marked. The solar wind observed by ACE at this time had a nominal dynamic pressure of 1.34 nPa and a southward interplanetary magnetic field component of about -2 nT.

2.2. Observations From Fort Smith

[13] An important component of the THEMIS mission to complement space observations is the ground-based observatory (GBO) network of all-sky-cameras (ASCs) [Mende *et al.*, 2008]. Keogram from Fort Smith (geographic latitude and longitude: 60.0°N and 248°E) and selected 1-min resolution of ASC auroral images during this interval are shown in Figure 2. The keogram indicates a brightening of auroral arc starting at 0714 UT and a very significant intensification subsequently. The ASC auroral images below the keogram show this development of brightening quite well. This onset was followed by a small poleward expansion of auroral activity. The auroral brightness faded substantially by 0729 UT. Careful examination of the keogram and the ASC image sequence indicates that there was an auroral arc poleward of the initial brightening arc. It remained undisturbed (i.e., no breakup-like activity) while the equatorward arc was expanding poleward. This observation is consistent with the well-known fact that the substorm expansion onset arc is typically the most equatorward one [Akasofu, 1964].

[14] A second auroral activation occurred with arc brightening and breakup at ~ 0742 UT followed by a poleward expansion. The auroral brightness and the amount of poleward expansion exceeded that of the first activation. Again, from the keogram and ASC images, there was an arc poleward of the brightening arc that remained undisturbed until the poleward expansion of the active arc reached that location. From ~ 0745 to ~ 0800 UT, bright aurora covered

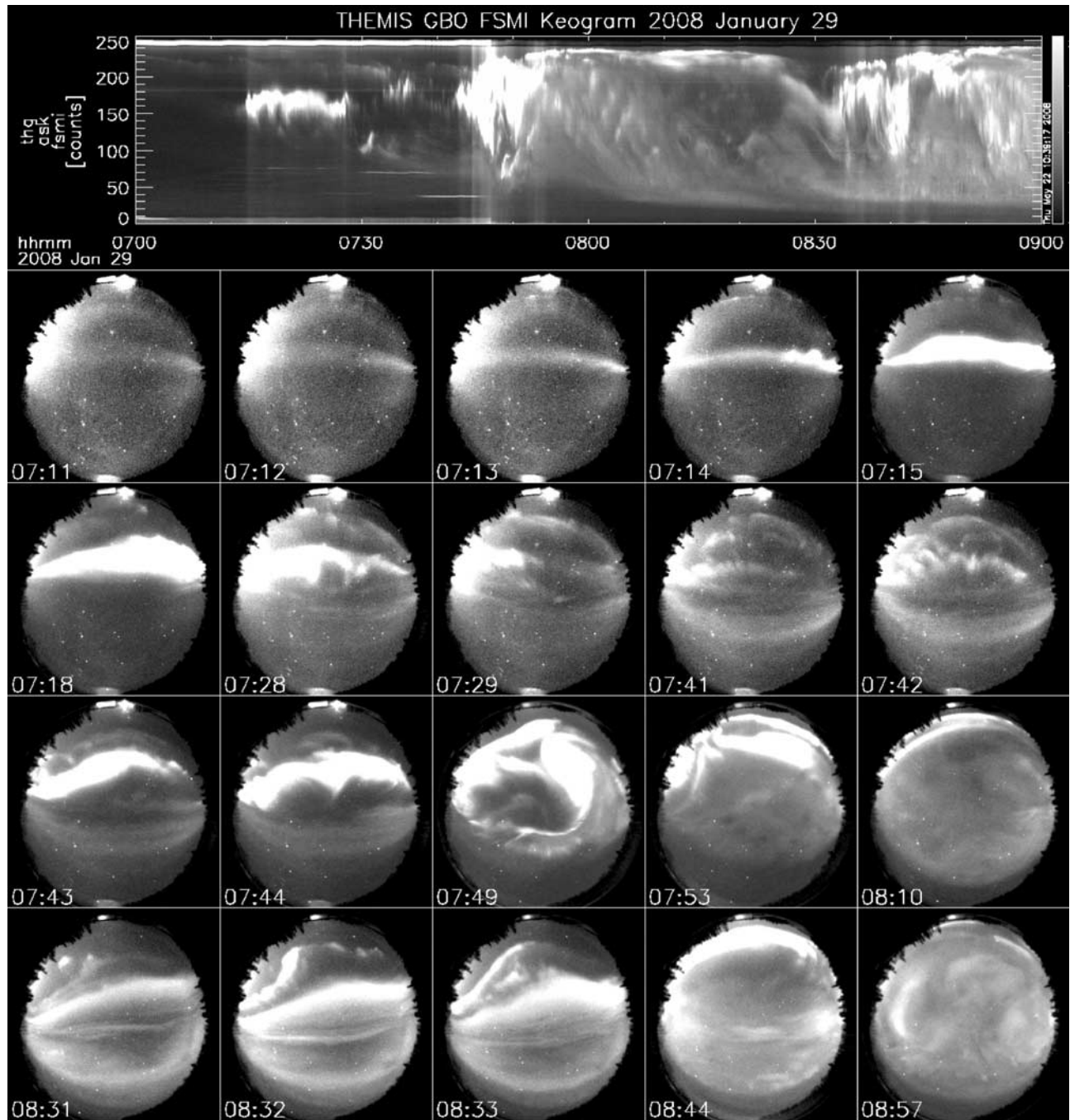


Figure 2. The keogram and selected sequence of 1-min resolution of all-sky-camera (ASC) auroral images from Fort Smith. In the ASC auroral image, north is upward and east is to the right. Three auroral activations with onsets at 0714, 0742, and 0832 UT can be identified. The first two onsets of initial brightening occurred equatorward of an auroral arc that did not show breakup activity.

the entire sky above the station. This pattern gradually changed to one that shows bright auroras in the poleward and equatorward portions with relatively dim brightness in between, most evident from ~ 0807 UT to ~ 0823 UT in the keogram. This pattern has the characteristics of a double oval [Elphinstone *et al.*, 1996], which is a common morphology in the late substorm expansion phase. The auroral activity started to recede equatorward at ~ 0824 UT.

[15] The ASC image at ~ 0831 UT shows an auroral arc extending from the west into the field-of-view. A minute

later, the auroral arc just equatorward of it started to brighten and later became the brightest feature in the sky. Interestingly, there was an auroral arc equatorward of this brightening arc. It did not brighten until ~ 0839 UT.

2.3. Observations From Fort Simpson

[16] To the west of Fort Smith is Fort Simpson (geographic latitude and longitude: 61.8°N and 239°E) with the ASC field-of-view partially overlapping that of Fort Smith. Figure 3 shows the keogram and selected 1-min resolution

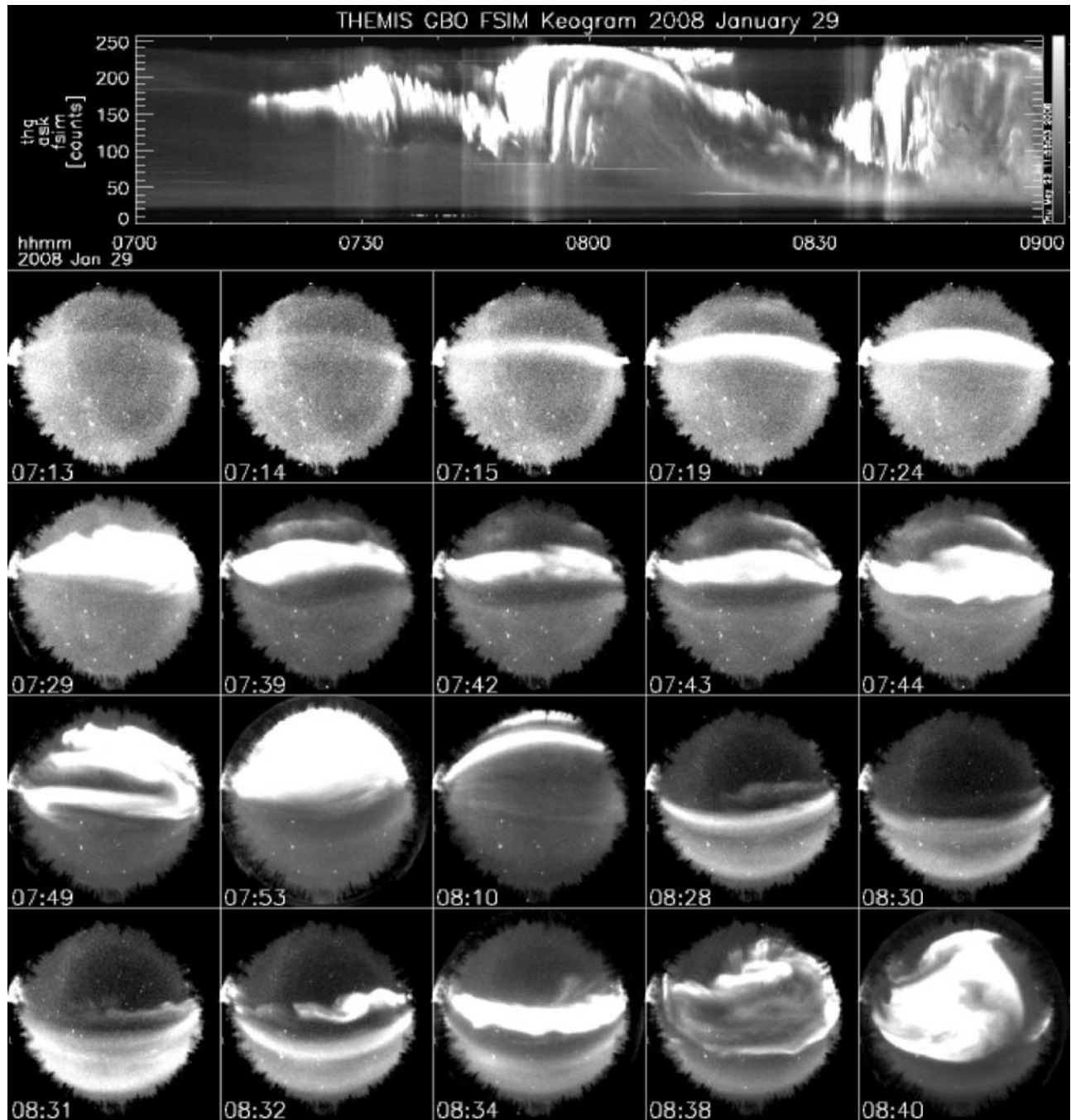


Figure 3. The keogram and selected sequence of 1-min resolution of ASC auroral images from Fort Simpson. Three auroral activations at the same times as identified at Fort Smith ASC images can be seen. The third activation occurred at the most poleward arc.

of ASC images from this station. Similar to the Fort Smith observation, an auroral arc brightened slightly from the east at 0714 UT, followed by significant brightening and poleward expansion. Careful examination of the ASC images indicates an auroral arc visible poleward of the brightening arc. This poleward auroral arc remained relatively undisturbed from ~ 0715 to ~ 0729 UT. By 0729 UT, the poleward expansion reached the location of the relatively undisturbed poleward arc. The overall auroral activity subsided substantially by 0739 UT.

[17] The activity resumed again at 0743 UT with significant brightening of the auroral arc near the zenith of the station. Again, there was a distinct auroral arc poleward of the brightening arc that remained relatively undisturbed until 0749 UT when the poleward expansion reached there. The activity subsided by 0826 UT when the auroral activity retreated equatorward to the southern portion of the sky at Fort Simpson.

[18] Another auroral activity started at 0831 UT when an auroral arc, poleward of the retreating auroral arc, expanded

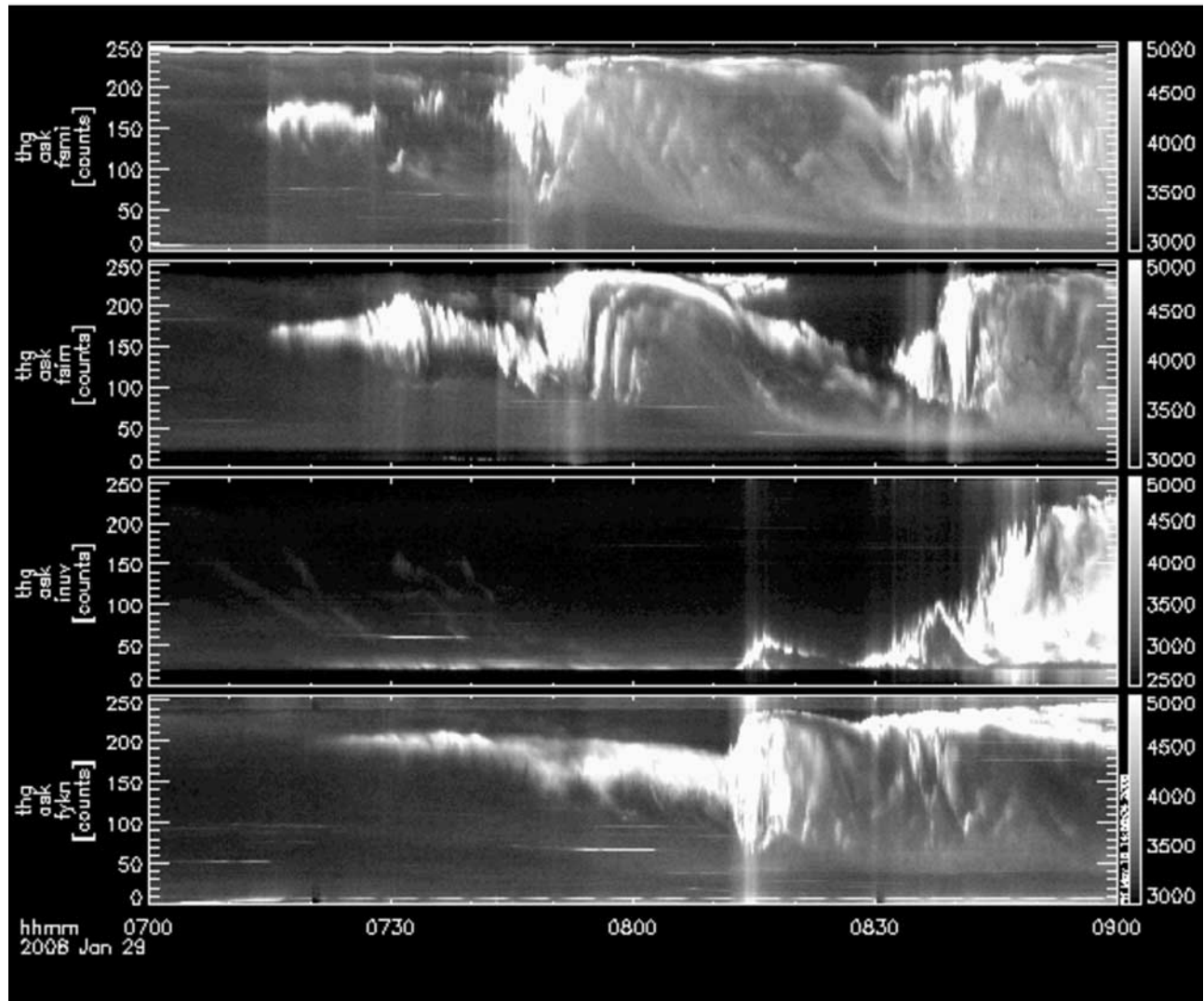


Figure 4. Keograms from Fort Smith, Fort Simpson, Inuvik, and Fort Yukon are shown from top to bottom. The third auroral activation seen at Fort Smith and Fort Simpson occurred later than at Inuvik and Fort Yukon, which was at 0828 UT.

from the east to the station. One minute later at 0832 UT, that arc started to brighten and eventually expanded poleward to form the auroral bulge, covering the entire sky of the station.

2.4. Observations From Inuvik and Fort Yukon

[19] To the northwest of Fort Simpson are Inuvik (geographic latitude and longitude: 68.4°N and 226°E) and Fort Yukon (geographic latitude and longitude: 66.6°N and 215°E) that showed considerable auroral activity, especially during the second half of the interval. Figure 4 shows the keograms from these two stations together with that from Fort Smith and Fort Simpson for comparison. The auroral activity that started at 0742 UT seen from Fort Smith eventually reached the local times and latitudes of Inuvik and Fort Yukon at a much later time (at ~0813 UT). The poleward expansion at these local times continued till ~0817 UT. Note that while aurora activity was retreating equatorward substantially during 0817–0829 UT at Fort Smith and Fort Simpson, the auroral activity at the local

times of Inuvik and Fort Yukon showed only slight equatorward retreat. Another activation started at ~0828 UT at Inuvik and Fort Yukon with subsequent poleward expansion. This activity was initiated at the poleward boundary of the auroral luminosity region and preceded the auroral activation at Fort Smith and Fort Simpson that started at ~0831 UT. Therefore, the local time of the first and second auroral activations was close to Fort Smith while that of the third auroral activation moved northwest to near Inuvik and Fort Yukon.

2.5. Summary of Ground-Based Observations

[20] To recapitulate, THEMIS GBO showed three major auroral activations during this interval. The first one started at ~0714 UT with a small poleward expansion. The second one started at ~0742 UT and had a major poleward expansion. The third one started at ~0828 UT and had a poleward expansion also. The first two activations were initiated near the equatorward portion of the visible aurora and there was an auroral arc poleward of the initial

Ground stations and projected satellite locations at 0800 UT

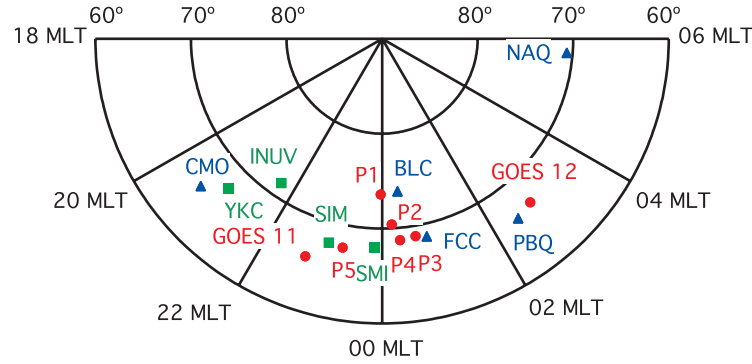


Figure 5. A map of ground stations and projected satellite locations at 0800 UT. The ground stations contributing to the AU/AL indices are marked by solid triangles. The THEMIS GBO stations used in this study are marked by solid squares. The projected satellite locations based on the T89 magnetic field model are marked by solid circles.

brightening arc that remained relatively undisturbed until the poleward expansion of the auroral bulge reached there. In contrast, the third activation was initiated near the poleward boundary of the auroral precipitation. The AU/AL indices indicate the occurrence of two substorms during this conjunction interval. The first one was an isolated substorm that started at ~ 0714 UT, matching the time indicated by the THEMIS GBO network. The second one was a moderate size substorm with several intensifications. Its onset was at ~ 0742 UT, again matching well with the onset time indicated by the THEMIS GBO network. The third auroral activation corresponds to an intensification of the continuous substorm activity initiated by the second auroral activation. The intensification onset time (third time mark in Figure 1b) is later than the onset of auroral activation at ~ 0828 UT from GBO ASC data because the continuous AL activity masks the precise onset of the intensification. Although not shown here, the global auroral images provided by Polar UVI corroborate the onset times of the first two auroral activations but miss the third one owing to the lack of data during that interval. Within the local times of 21 MLT to 03 MLT, Polar UVI images also confirm that the first substorm activity was localized mostly to the postmidnight sector while the second substorm activity spanned over a wider local time sector than the first.

3. Satellite Observations

[21] In this section, we present a general overview of representative observations from four THEMIS satellites. It is appropriate to mention the approximate footprints of the THEMIS and GOES satellites in order to relate satellite observations to ground activity. The projections of these satellite locations along magnetic field lines based on the T89 magnetic field model at 0800 UT are shown in Figure 5, together with the ground stations. Note that the locations of the ground stations at different UT from 0800 UT will be rotated according to the UT time, to the left (right) for earlier (later) UT time. Figure 5 shows the satellite footprints to be well embedded within the coverage of the ground stations. THEMIS C, D, and E were located slightly to the east portion of sky covered by Fort Smith. THEMIS

A was located between Fort Smith and Fort Simpson. The projection locations do not change much with the T96 magnetic field model. These projected locations may not be precise since the magnetic field models used to perform the projections may be unreliable during substorm intervals. However, they can be used as a rough guide and provide probably fairly accurate information about their locations relative to each other on the ground.

3.1. Observations From THEMIS D

[22] An overview of THEMIS D observations during this interval is shown in Figure 6. THEMIS D was at $\sim 11 R_E$ downstream, in the middle of the line of THEMIS satellites. Data from the top to the bottom panels are the ion energy spectrum from SST (D. Larson, private communication, 2008), ion energy spectrum from ESA [McFadden *et al.*, 2008], electron energy spectrum from SST, electron energy spectrum from ESA, anisotropy of energetic ions from SST (90° , 0° , and -90° refer to particles going duskward, sunward, and dawnward, respectively; the plus symbols show the projections of the magnetic field on the spin plane), power spectrum of wave electric field from EFI [Bonnell *et al.*, 2008; Cully *et al.*, 2008], power spectrum of wave magnetic field from SCM [Roux *et al.*, 2008], ion velocity components from ESA, and magnetic field components from FGM [Auster *et al.*, 2008].

[23] There are three notable dipolarizations indicated well in the bottom panel by the B_z trace. These dipolarizations are associated with high variations in all magnetic field components and significant plasma flows. For the first dipolarization at ~ 0714 UT, the ion energy spectra show ion energization. On the other hand, the electron energy spectra indicate an increase in energy flux for the energetic (SST) electrons simultaneous with a decrease in energy flux for the low-energy (ESA) electrons. Sunward anisotropy of energetic ions, i.e., particles going sunward, is indicated in the anisotropy panel. The wave panels indicate significant wave activity in the electric and magnetic components during dipolarization, extending in frequency to ~ 1 kHz in the electric component and to ~ 100 Hz in the magnetic component. Accompanying the dipolarization were significant plasma flows. Before and during the early part of

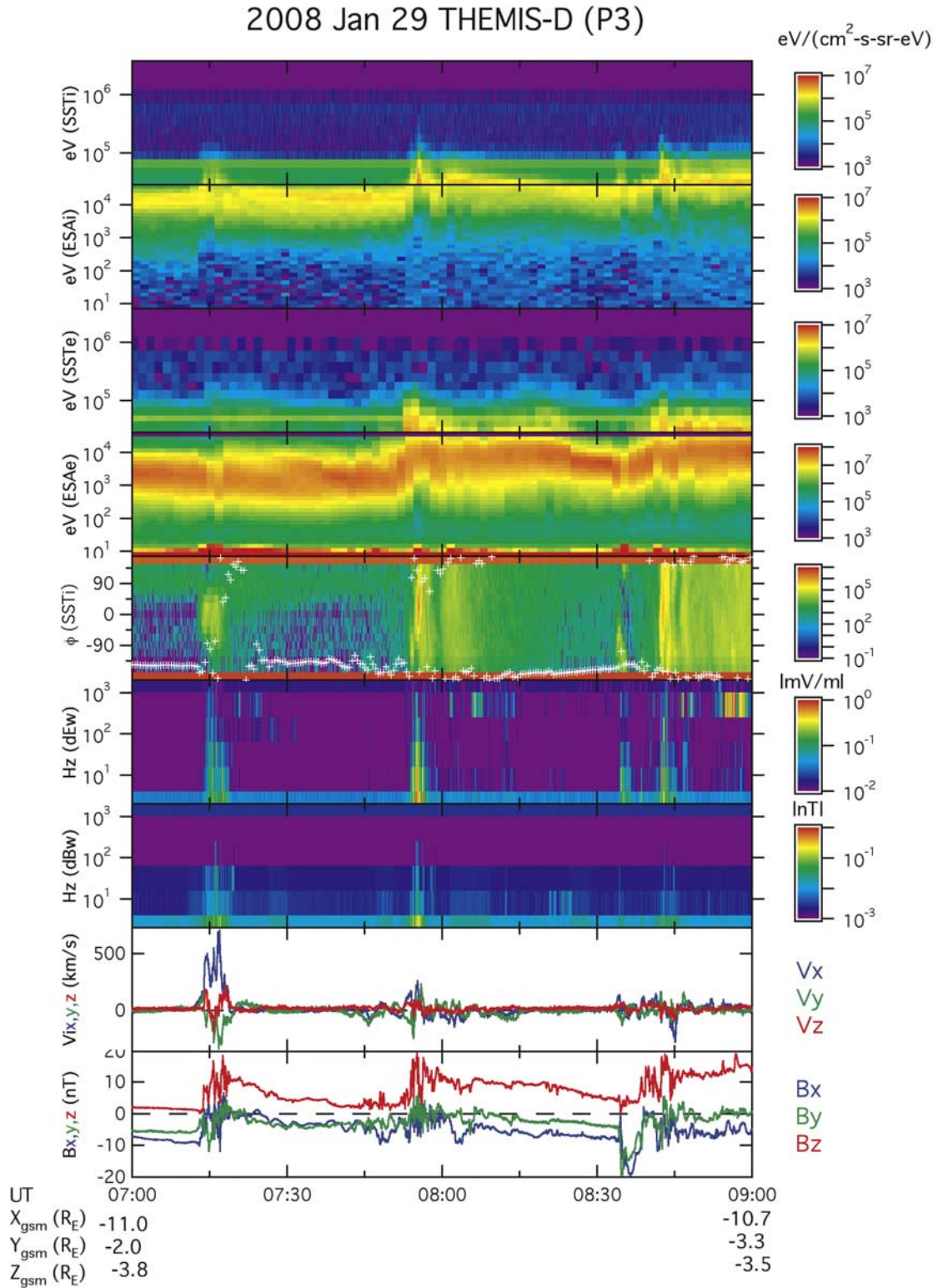


Figure 6. Overview of observations from THEMIS D (P3). The colors used in the labels for the velocity and magnetic field panels indicate the different components in these panels. The unit given on the left label for particle energy spectrum is eV, and that for the wave power is Hz. In the anisotropy spectrogram, the sectors at 0° and at -135° had high background levels and are replaced by the geometric mean of the flux levels at adjacent sectors. In addition, the two sectors corresponding to particles going tailward (sectors at the bottom and top of the panel) showed artificially high flux levels and should be ignored. Three dipolarizations with large magnetic field fluctuations can be seen, corresponding to the three auroral activations seen by the THEMIS ground-based observatory stations.

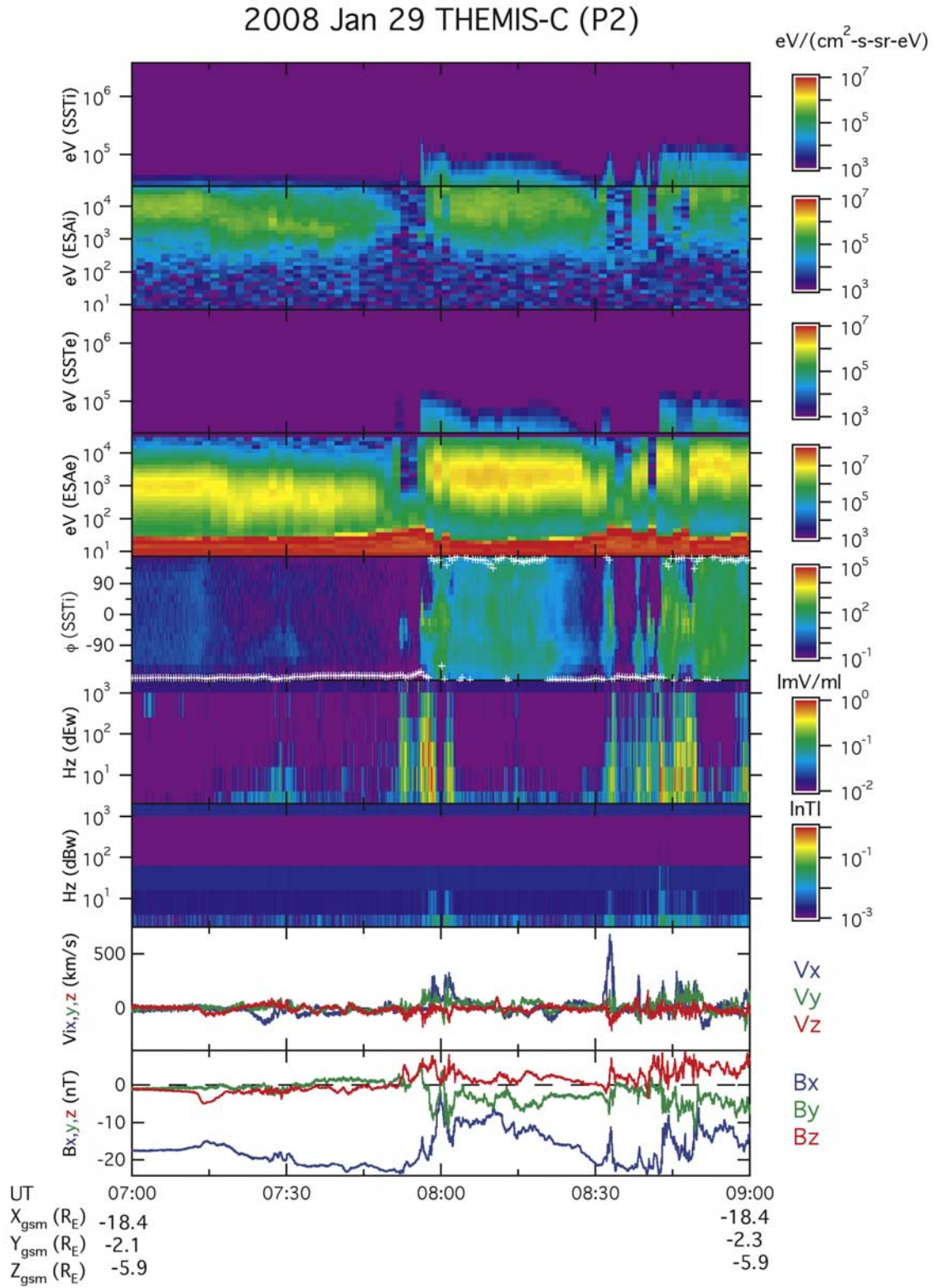


Figure 7. Overview of observations from THEMIS C (P2). Only two substorm disturbances corresponding to the second and third auroral activations were seen clearly at this midtail location.

dipolarization, $V_x > 0$ (earthward) and $V_y > 0$ (duskward). Although $V_y < 0$ (dawnward) later, dipolarization was not due to activity duskward of the satellite location since the Polar global UVI images indicate auroral activity being

mostly in the postmidnight sector and dipolarization at GOES 12 in the postmidnight sector was larger than that at GOES 11 in the premidnight sector (see Figure 10). During the interval of high fluctuations in the magnetic field

components, the B_z component had the largest magnitude and the B_x component was small in general, indicating that the satellite was close to the neutral sheet.

[24] The second dipolarization was associated with significant particle energization in both ions and electrons. The energetic ions showed slight downward anisotropy (-90°) first, followed by sunward and duskward anisotropy (22.5°). This is consistent with the particle energization front expanding eastward first and moving over the satellite subsequently. The wave powers at both electric and magnetic components were higher than that of the first activation. On the other hand, the plasma flows were slower. The V_x and V_y components had mainly positive values but reversed in sign briefly during dipolarization. Magnetic field fluctuations occurred in all three components. Similar to the first dipolarization, in general the B_z component had the largest magnitude among the components.

[25] Similar characteristics of particle, field, and wave activity can be seen for the third dipolarization. However, there are some differences as well. At ~ 0834 UT prior to dipolarization, the B_x and B_y components showed significant negative excursions, simultaneous with dawnward anisotropy of energetic ions and start of particle energization. The ion anisotropy later became sunward-duskward. This is consistent with the energization front expanding eastward over the satellite as mentioned before. Tailward plasma flows appeared in the later part of the dipolarization interval.

[26] In terms of magnetic fluctuations, it is found that its magnitude decreased with increasing distance from the neutral sheet. This trend indicates that magnetic fluctuations are most prominent near the neutral sheet. The enhancement of magnetic fluctuations, mostly below 4 Hz (around the proton cyclotron frequency), is in agreement with the earlier report by *Le Contel et al.* [2008] on the intensification of these waves during dipolarizations and substorm activity on 23 March 2007. They concluded that these waves might play a significant role in plasma transport and energization during substorms [*Le Contel et al.*, 2001]. *Lui et al.* [1991] have considered these magnetic fluctuations to be signatures of waves generated by the cross-field current instability that causes current disruption and dipolarization.

[27] Overall, although there are three dipolarizations occurring close in time, each one had the particle, field, and wave characteristics quite distinct from each other. These differences suggest that the observed characteristics depend sensitively on the observing site relative to the location where dipolarization is initiated.

3.2. Observations From THEMIS C

[28] Tailward of THEMIS D was THEMIS C, which was in the midtail at $18.4 R_E$ downstream during this interval. Figure 7 shows an overview of THEMIS C observations. The meaning of the anisotropy direction is different from Figure 6: 90° and -90° imply particles going downward and duskward, respectively, due to the fact that the spin axis of THEMIS C points south whereas that of THEMIS D points north.

[29] The magnetic field panel indicates that there was no dipolarization seen for the first auroral activation. This lack of activity indicates the first auroral activation to be a spatially localized disturbance in the magnetotail. At

~ 0713 UT, about 1 min before the onset time of the first auroral activation, the B_z component started a southward excursion while the B_x component was still larger than the B_z component. There was no significant V_x or V_y accompanying this southward dipping.

[30] For the second auroral activation at ~ 0742 UT, there was no significant change at first. However, plasma dropout soon followed (~ 0751 – 0757 UT). This dropout was not associated with compensating increases in the magnitudes of the B_x and B_y components, suggesting a lack of pressure balance at this time. During this dropout, brief duskward anisotropy of energetic ions were detected. This is probably due to flapping of the plasma sheet and its edge was detected through the large ion gyroradii of energetic ions. The detection of the boundary was accompanied by significant power in the wave electric field. At the plasma sheet recovery, there were significant increases of the B_z component with sunward plasma flows and sunward anisotropy of energetic ions. There was significant wave activity with this reentry. The activity subsided slightly and then repeated itself again at ~ 0801 UT.

[31] Similar activity developed for the third auroral activation. These include very brief plasma dropouts (~ 0832 – 0836 UT and ~ 0841 UT), bursty earthward plasma flows, sunward anisotropy of energetic ions, multiple increases and decreases of the B_z component, and multiple bursts of wave power. Plasma sheet recovery eventually reached the satellite location.

3.3. Observations From THEMIS A

[32] The innermost THEMIS probe at this time was A, located at ~ 8 to $9 R_E$ downstream during this interval. An overview of its observations is shown in Figure 8. The spin axis of THEMIS A points north and so 90° in the anisotropy plot means ions going duskward.

[33] The magnetic field panel indicates two prominent dipolarizations associated with the last two auroral activations. For the first auroral activation at ~ 0714 UT, there was almost no sign of activity at this location. The energy spectra of ions and electrons show increases of energy flux in the lower energy range. There was no plasma flow associated with this change in energy spectra. Later at ~ 0718 UT, there was a decrease in the B_z component, again without any accompanying plasma flows. This B_z decrease may be a spatial change as the satellite moved further downstream to a more tail-like configuration. The lack of activity for the first auroral activation suggests that the corresponding disturbance in the tail was spatially localized also in the near-Earth region in addition to the midtail region as discussed in section 3.2.

[34] In contrast to the first auroral activation, drastic changes occurred at the second auroral activation. There was a very sharp energization of ions and electrons associated with dipolarization at ~ 0745 UT. The magnetic field components exhibited large variations with the dipolarization. The anisotropy of energetic ions was predominantly duskward at the start of particle energization. There was significant power in the wave electric and magnetic fields associated with particle energization.

[35] For the third auroral activation at ~ 0828 UT, dipolarization occurred at ~ 0841 UT, considerably later than the auroral activation and preceded by a brief (~ 1 min) decrease

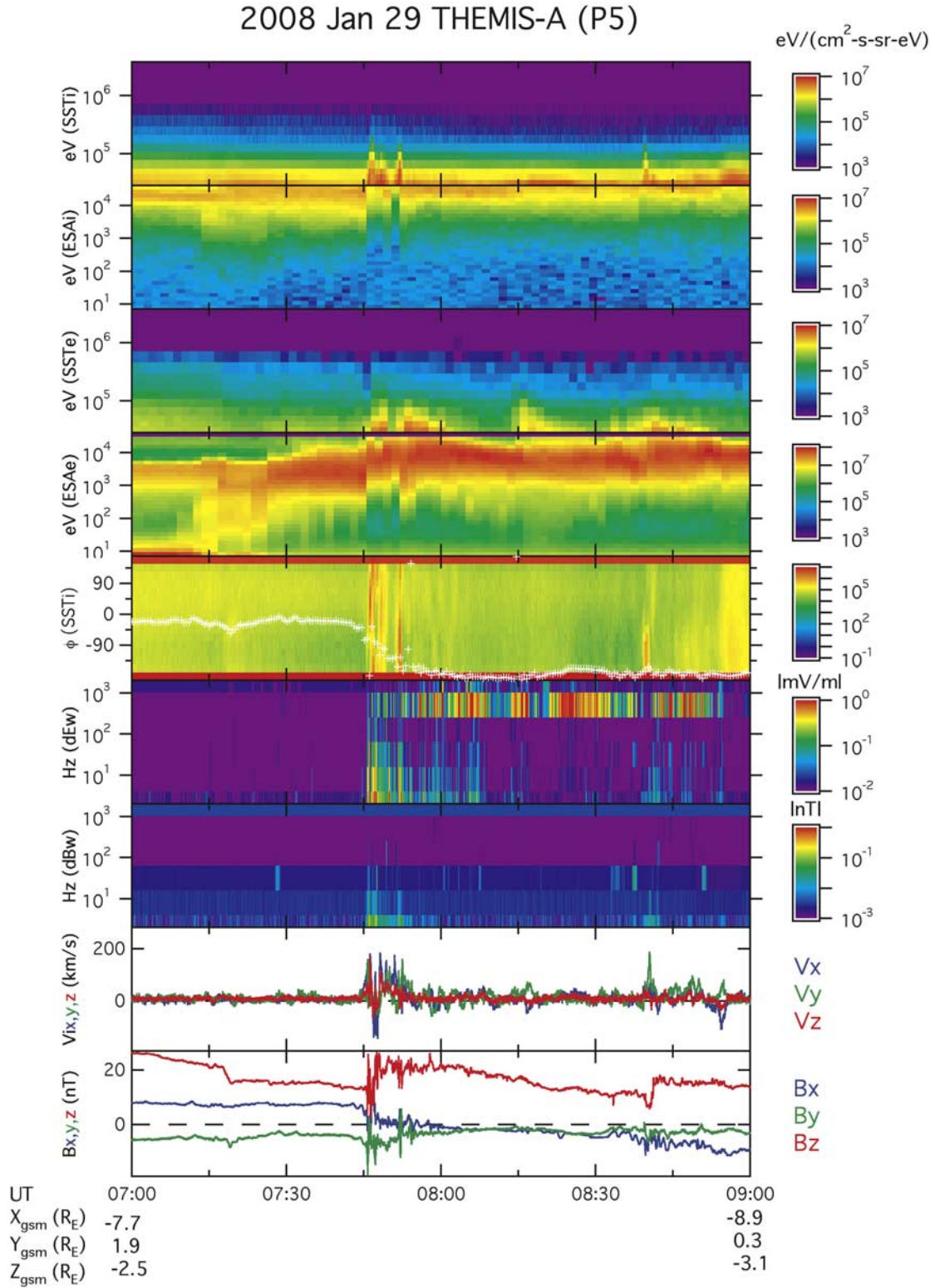


Figure 8. Overview of observations from THEMIS A (P5). Similar to THEMIS C, only two substorm disturbances were seen clearly at this location.

of the B_z component. Not much magnetic field fluctuations were seen. Plasma flows were mainly downward, so was the anisotropy of energetic ions. There was evidence of some energization of ions and electrons as well as some enhancements in the wave activity.

3.4. Observations From THEMIS B

[36] THEMIS B at this time was the outermost satellite, located at $\sim 30 R_E$ downstream during this period. Figure 9 shows an overview of its observations. The spin axis of

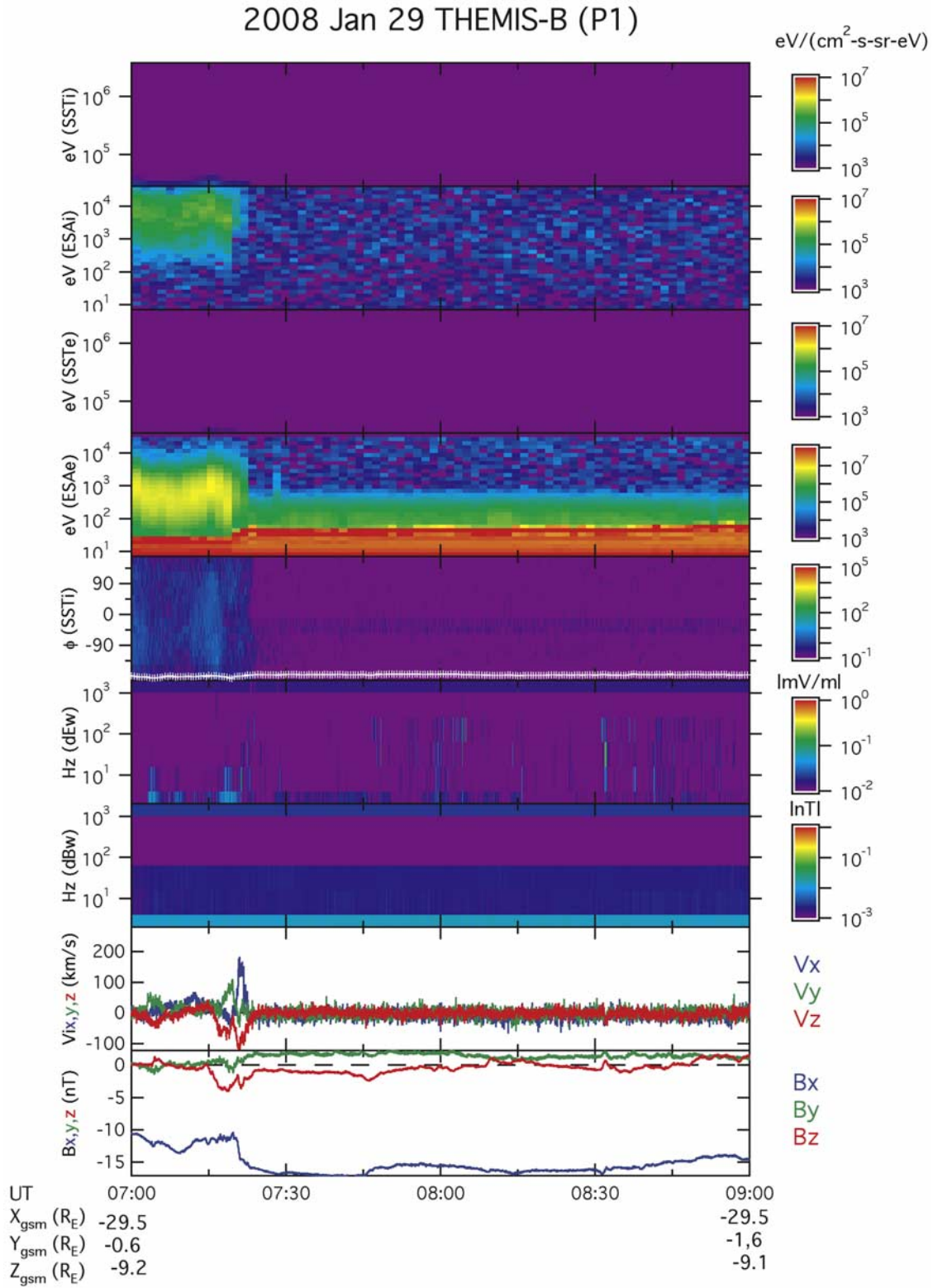


Figure 9. Overview of observations from THEMIS B (P1). Plasma sheet thinning was seen after the first auroral activation at this location, causing the satellite to exit to the tail lobe.

THEMIS B points south and so 90° in the anisotropy plot means ions going downward.

[37] The satellite was in the high-latitude plasma sheet at the beginning, with the B_x magnitude much larger than the

B_z magnitude. Near the time of the first auroral activation, southward excursion of the B_z component was seen, accompanied mainly by earthward plasma flow. The earthward flow was mainly along the magnetic field in the

plasma sheet boundary layer. The satellite exited the plasma sheet soon after the detection of this plasma flow and remained in the tail lobe for the rest of the interval. A slight southward dipping was observed around the time of the second auroral activation, in spite of the fact that it was in the tail lobe. There was no strong anisotropy of energetic ions seen and the wave activity appearing in the electric field component was low.

4. Time History of Substorm Development in the Magnetotail

[38] In this section, we take a closer look at the satellite observations for the three auroral activations. The time history of substorm development is assessed by comparing the onsets of substorm disturbances at different locations in the magnetotail.

4.1. First Auroral Activation at 0714 UT

[39] Figure 10 shows measurements of the B_z component in GSM from the five THEMIS satellites and the two GOES satellites, and the V_x component of plasma ion flow from the five THEMIS satellites. Different ranges in the ordinate axes are used to accommodate the large differences in the magnitude of parameters at different tail locations. The vertical dashed lines denote the three auroral activation times seen by the GBO network.

[40] Increases in the B_z component associated with the auroral activation at ~ 0714 UT were seen as dipolarization onsets by THEMIS D and E and the two GOES satellites. The dipolarization at GOES 11 is less noticeable because of the large range used in the ordinate axis but it is still significant. The increase in the B_z component was larger at GOES 12 than at GOES 11, suggesting that GOES 12 was closer to the substorm onset location (consistent with the Polar UVI global auroral observations that the first auroral activation was mostly in the postmidnight sector). In contrast, decreases in the B_z component were observed by THEMIS A, B, and C. The earliest B_z decrease occurred at THEMIS C, followed by B, and finally by A. The negative excursions of B_z for THEMIS B and C are southward dipping of the magnetic field related to plasma sheet thinning at these downstream distances during the early substorm expansion phase as described by Hones [1979]. In addition, THEMIS B observed a small bipolar signature prior to southward dipping. In terms of temporal development, plasma sheet thinning signature was first observed by THEMIS C at $-18 R_E$ just about the substorm expansion onset time. The thinning proceeded downstream and was observed by THEMIS B at $-30 R_E$ about 2 min later. THEMIS B exited the plasma sheet boundary at ~ 0723 UT after detecting moderate plasma flows at the plasma sheet boundary layer as discussed in section 3.4. Therefore, plasma sheet thinning for this substorm proceeds from the near-Earth region to the midtail. This thinning is probably not drastic enough to trigger current disruption in the midtail during the early substorm expansion phase.

[41] Weak earthward plasma flows ($< \sim 150$ km/s) were detected prior to dipolarizations at THEMIS D and E. Even though D and E were very close to each other ($\Delta x \sim 0.2 R_E$, $\Delta y \sim 1.0 R_E$, and $\Delta z \sim 0.1 R_E$), there are noticeable differences in the B_z temporal profile and major differences in the

V_x temporal profile. These differences emphasize the spatially localized nature of dipolarization and its associated plasma flows. At THEMIS C, there was no significant V_x and V_y associated with southward dipping of the magnetic field. However, weak tailward plasma flows occurred later at ~ 0723 UT.

[42] From the onset times of magnetic field changes, plasma flows, and particle energization at the seven locations in the magnetotail, this auroral activation corresponds to substorm disturbance initiated in the downstream distance between THEMIS D and C, i.e., $X_{GSM} \approx -11$ to $-18 R_E$. Since the onsets of various substorm activities at THEMIS D were simultaneous with the ground auroral activation and were earlier than those at THEMIS C, the substorm initiation location was probably closer to THEMIS D than to THEMIS C. Furthermore, there was an auroral arc poleward of the initial brightening arc that remained undisturbed (Figures 2–4), indicating that the substorm activity never reached the poleward boundary of the auroral oval. Therefore, this substorm did not involve magnetic reconnection on open magnetic field lines. This implication has been pointed out previously from ground observations [e.g., Lyons *et al.*, 2002] and from an early THEMIS event during the commissioning phase without the operation of onboard plasma instrument by Donovan *et al.* [2008]. The additional new information reported here are the simultaneous space observations (including plasma measurements) along the tail axis extending to $\sim 30 R_E$ downstream distance with this auroral feature seen from the ground. The MTI model predicts dipolarization to be intimately linked to earthward plasma flow through magnetic flux transport. Therefore, earthward plasma flow should occur prior to dipolarization, earlier in the midtail than in the near-Earth location since magnetic flux is to be moved from the midtail to the near-Earth region. The absence of significant earthward plasma flow at THEMIS C and the lack of significant earthward plasma flow prior to and during dipolarization at THEMIS E are therefore inconsistent with the MTI model.

4.2. Second Auroral Activation at 0742 UT

[43] The first indication of substorm activity for the second auroral activation was recorded at ~ 0746 UT by THEMIS A which detected large fluctuations in the B_z component and significant earthward plasma flows. THEMIS A was the innermost probe of all THEMIS satellites (see Figure 1). THEMIS B, the outermost probe, was in the tail lobe and detected a slight southward dipping of the magnetic field after auroral activation onset. Simultaneously, THEMIS E observed moderate tailward flows accompanied by small increases in the B_z component. Since the tailward flows occurred with northward magnetic field, the observed tailward flows are unlikely to be caused by a magnetic reconnection site earthward of THEMIS E. THEMIS D also observed weak tailward flows when dipolarization occurred at THEMIS A, followed by some bursts of earthward flows. During these flow activities, THEMIS D observed some transient positive excursions of B_z first and the larger increases of B_z occurred later at ~ 0752 UT, nearly simultaneous with the dipolarization at THEMIS C and the onset of Pi2 pulsations (~ 100 s period) in the B_z component at GOES 12. It may be noted that the dipolarization at THEMIS C was not accompanied by any plasma flow.

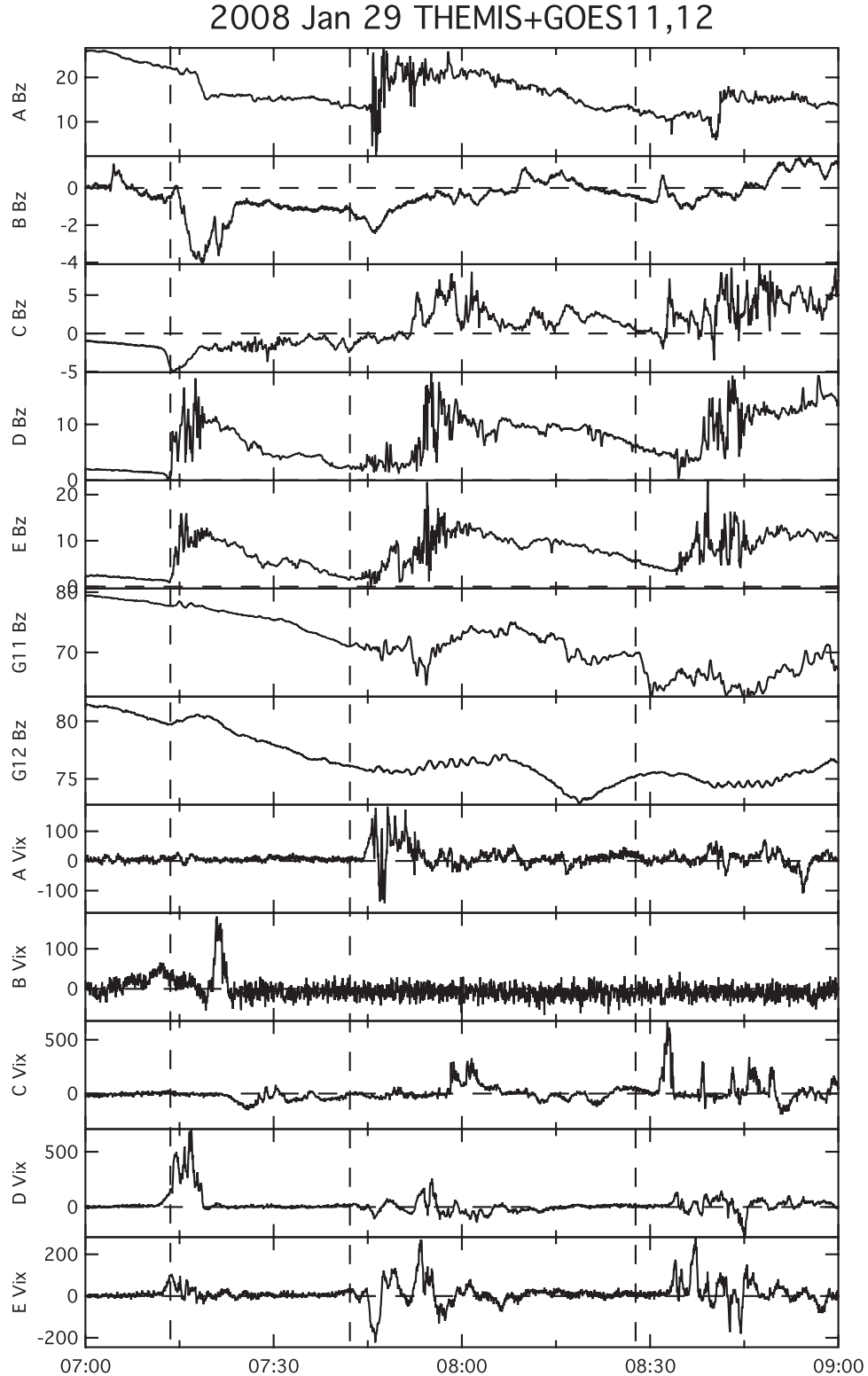


Figure 10. Observations of the northward component of the magnetic field from THEMIS satellites, GOES 11, and GOES 12 together with the V_x component of the plasma flow from THEMIS satellites. Comparison of onset times of dipolarizations, plasma flows, and particle energization among these satellites indicates that the substorm onset location was between THEMIS D and C ($X_{\text{GSM}} \approx -11$ to $-18 R_E$) for the first auroral activation, between THEMIS A and D ($X_{\text{GSM}} \approx -8 R_E$ to $-11 R_E$) for the second auroral activation, and tailward of THEMIS B (at $X_{\text{GSM}} \approx -30 R_E$) for the third auroral activation.

However, this lack of flow signature may be due largely to the fact that almost the entire ion population was outside the energy range of ESA (see Figure 7). Indication of dipolarization at GOES 11 came at ~ 0747 UT, shortly after dipolarization at THEMIS A and significantly earlier than the onset of Pi2 pulsations at GOES 12 (~ 0750 UT). The time delay between these two GOES satellites is likely due to eastward expansion of the substorm disturbance.

[44] The anisotropies of energetic ions observed by SST in all THEMIS satellites during 0745–0800 UT are shown in Figure 11. Note that 90° marks the duskward streaming direction for THEMIS A, D, and E whereas -90° marks that for THEMIS B and C. THEMIS A detected an increase in energetic ions first at ~ 0746 UT and these ions had duskward anisotropy. THEMIS D and E detected the flux increase at ~ 0754 UT. Apart from a transient flux increase which corresponds to the detection of the plasma sheet boundary layer through the large gyroradii of energetic ions as discussed in section 3.2, THEMIS C detected the flux increase at ~ 0756 UT later than THEMIS D and E. THEMIS B was in the tail lobe and did not detect any energetic ion flux for this interval.

[45] Overall, the time history of substorm disturbance based on onset times of magnetic field changes, plasma flows, and enhanced energetic ion fluxes indicates substorm onset originated in the near-Earth plasma sheet between THEMIS A (at $X_{\text{GSM}} \approx -8 R_E$) and THEMIS D (at $X_{\text{GSM}} \approx -11 R_E$). Since earthward plasma flow occurs at THEMIS A before THEMIS D, this time sequence of earthward plasma flow is consistent with the NEI model and not with the MTI model. In addition, the lack of significant earthward plasma flow prior to dipolarizations at THEMIS D and E is also inconsistent with the MTI model. Furthermore, the lack of disturbance on the auroral arc poleward of the initial brightening arc until the brightening reached the arc location (Figures 2–4) indicates that the substorm onset did not involve magnetic reconnection on open magnetic field lines for a substantial time interval after onset.

4.3. Third Auroral Activation at 0828 UT

[46] Returning back to Figure 10, one may see the earliest indication of substorm disturbance for the third auroral activation to be at THEMIS C. The observed changes include dipolarization accompanied by strong earthward plasma flow up to ~ 700 km/s. There were several intermittent flow bursts afterward, separated in time by ~ 2 – 5 min. The B_z component was slightly negative just before the dipolarization but no tailward plasma flow was seen to accompany the negative B_z occurrence. THEMIS B was in the tail lobe still. Nevertheless, southward dipping of the magnetic field was observed at about the same time as dipolarization was observed at THEMIS C. Dipolarization and plasma flow activity came later at THEMIS D and E. The latest dipolarization was seen at THEMIS A accompanied by weak earthward plasma flows. Except for the occurrence of Pi2 pulsations starting at ~ 0840 UT at GOES 12, there was no clear indication of substorm disturbances at GOES 11 and 12 for this auroral activation, suggesting that this activation did not affect the geostationary altitude significantly even though THEMIS C detected strong earthward plasma flow. This result is consistent with the

statistical result reported by Ohtani *et al.* [2006] that dipolarization at the geostationary altitude rarely occurs following fast earthward flow in the plasma sheet. The time history of these substorm signatures at different downstream distances is consistent with substorm disturbances originated tailward of THEMIS B at $\sim 30 R_E$ in the magnetotail.

5. Summary and Discussion

[47] We have investigated in detail a major tail conjunction of THEMIS on 29 January 2008 in the time interval of 0700–0900 UT. The observations from THEMIS satellites are complemented in space by GOES 11 and 12 and on the ground by THEMIS GBO all-sky-camera observations and AU/AL indices. Global UVI images from Polar are also available. This THEMIS major conjunction covers radial distances from the geosynchronous altitude to $\sim 30 R_E$ in the magnetotail. The period covers a small isolated substorm and a moderate size substorm, consisting of three auroral activations from THEMIS GBO data.

5.1. First Substorm

[48] For the first auroral activation that corresponds to the onset of an isolated substorm, the time history of substorm disturbances along the tail axis is consistent with the onset location in the near-Earth plasma sheet. The presence of a relatively undisturbed auroral arc poleward of the initial brightening arc indicates that the substorm activity did not reach the poleward boundary of the auroral oval. This indicates the absence of magnetic reconnection on open magnetic field lines. Even though negative B_z was observed at THEMIS C (at $X_{\text{GSM}} \approx -18 R_E$) near substorm onset time, it is unlikely to be a signature of magnetic reconnection for the following reasons. First, there was no tailward plasma flow associated with the southward dipping of the magnetic field. Second, there was no indication of tailward streaming of energetic electrons, an expected feature for magnetic reconnection located earthward of the satellite. Third, there was no signature in the B_y component indicative of the quadruple magnetic perturbations associated with magnetic reconnection. Fourth, THEMIS B (at $X_{\text{GSM}} \approx -30 R_E$) observed southward dipping of the magnetic field and earthward plasma flow, which is a combination inconsistent with magnetic reconnection occurring earthward of THEMIS B. Furthermore, when it exited the plasma sheet shortly after substorm onset, it did not detect tailward streaming of energetic electrons either. Therefore, there was no signature of magnetic reconnection at the plasma sheet boundary, consistent with the presence of an undisturbed auroral arc at the poleward boundary of the auroral oval for this auroral activation.

[49] The observations alone cannot rule out the occurrence of magnetic reconnection on closed magnetic field lines during this substorm, which is a possible variant from the traditional model invoking midtail initiation with magnetic reconnection on open magnetic field lines. However, one may consider the possibility of magnetic reconnection on closed field lines to account for the large plasma flow (up to ~ 700 km/s) seen at the inner probe THEMIS D for this auroral activation. The plasma flow in the outflow region of magnetic reconnection v_{out} is given by $v_{\text{out}} = \varepsilon B_0 / \sqrt{\mu_0 \rho_n}$, where ε is the reconnection rate, B_0 is the magnetic field in

2008 January 29 Anisotropy of SST 40-300 keV Ions

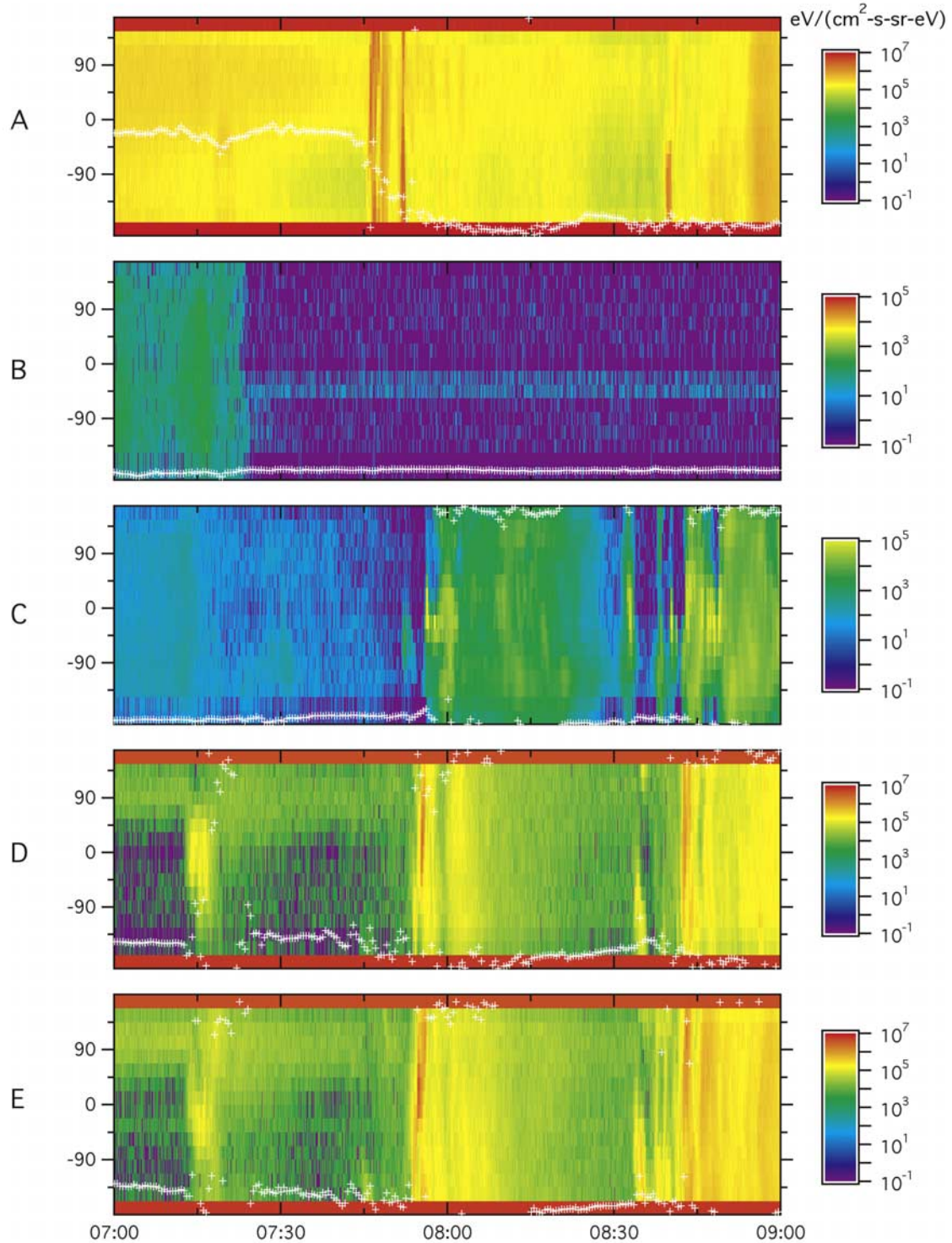


Figure 11. Anisotropy spectrograms of 40–300 keV energetic ions from THEMIS satellites during the second auroral activation interval. The anisotropies are projected to the spin plane of the satellites, which are approximately the GSE equatorial plane. The magnetic field direction projected on this plane is indicated by the plus symbol. Sectors at 0° for THEMIS A, D, and E, at -157° for THEMIS B and C, and at -123° for THEMIS D are contaminated and are replaced by the geometric mean of adjacent sectors. Sectors at -180° and at 157° for THEMIS A, D, and E are contaminated and should be ignored.

the inflow region, μ_o is the permeability of free space, and ρ_n is the mass density of the outflow region. The typical reconnection rate is given by $B_n/B_o \sim 0.1-0.2$, where B_n is the magnetic field normal to the current sheet in the outflow region. Since the magnetic field at the plasma sheet boundary was only ~ 15 nT, the magnetic field in the inflow region cannot exceed 15 nT for magnetic reconnection on closed field line well within the plasma sheet boundary. Also, the number density near the neutral sheet at THEMIS D is 0.4 cm^{-3} and in the plasma sheet boundary at THEMIS C is 0.3 cm^{-3} . The lowest number density for the v_{out} expression constrained by these observations is 0.3 cm^{-3} , which gives the maximum outflow speed of $\sim 60-120 \text{ km/s}$, far too low to account for the $\sim 700 \text{ km/s}$ observed by THEMIS D. Therefore, magnetic reconnection on closed field line can be ruled out on this basis. It is relevant to point out that even magnetic reconnection on open field lines does not necessarily produce a substorm, as demonstrated in two events reported by *Ohtani et al.* [2002].

5.2. Second Substorm

[50] For the second auroral activation, the time history of substorm disturbances along the tail axis is consistent with the substorm onset location between THEMIS A and D ($X_{\text{GSM}} \approx -8$ to $-11 R_E$). The time delay of activity at THEMIS C relative to that at THEMIS D and E is unlikely to be caused by eastward expansion of the substorm activity. From the projected locations, an eastward expansion would predict time delays at THEMIS D and E relative to THEMIS C, just opposite to the observed time sequence. Therefore, the time delay seen at THEMIS C arises from radial spreading and not from local time expansion of substorm disturbance. There was also an auroral arc poleward of the initial brightening arc that remained relatively undisturbed until the auroral bulge reached that arc, indicating that the onset did not involve magnetic reconnection on open magnetic field lines. Again, the observations alone cannot rule out the occurrence of magnetic reconnection in the closed field line region. However, the proximity of the onset location to the Earth ($X_{\text{GSM}} \approx -8$ to $-11 R_E$) suggests that it is highly unlikely for magnetic reconnection to occur owing to the strong positive B_z contribution from the Earth's dipole field in this region. Furthermore, if the outflow speed from magnetic reconnection on closed field lines is weak, then it is unlikely to reach the inner probe THEMIS A at $\sim 8 R_E$ in the tail.

5.3. Substorm Intensification of the Second Substorm

[51] For the third auroral activation, the brightening arc was located near the poleward boundary of the auroral oval and the time history of substorm disturbances along the tail axis is consistent with activity initiated tailward of $X_{\text{GSM}} \approx -30 R_E$. Since this activity occurred during the continuation of the activity initiated by the second auroral activation and the arc brightening was near the poleward boundary, it is considered to be a substorm intensification rather than an onset of another substorm expansion.

[52] One may still consider the possibility of this intensification as another substorm onset. First of all, there was no dipolarization seen at GOES 11 and 12 for the auroral activation at 0828 UT. In other words, if this were another substorm onset, it had no dipolarization at the geostationary

altitude, lacking a classic signature of substorm onset. Even the weak substorm onset at 0714 UT had dipolarization at the geostationary altitude as seen by GOES 11 and 12 (Figure 10). On the basis of the auroral development shown in the keograms in Figure 4, if there were another substorm onset after 0742 UT, it would have been 0813 UT rather than 0828 UT, with the former followed by a more significant poleward expansion than the latter. Given these observational facts, it is highly unlikely that the auroral activation at 0828 UT is qualified to be another substorm onset.

5.4. Time History Evaluation

[53] The time history of these three auroral activations observed during this THEMIS major conjunction interval can be summarized as follows. The onset times of magnetic field changes, plasma flows, and particle energization at the seven locations in the magnetotail indicate that substorm activity, including the occurrence of plasma flow, proceeds from the near-Earth region to the midtail for the first two auroral activations (substorm expansion onsets) but the time sequence reverses for the third auroral activation (a substorm intensification). Since the NEI model predicts that substorm onset activity, including the occurrence of plasma flow, proceeds from the near-Earth region to the midtail while substorm intensification activity can have the reverse time sequence, the observations of these two substorms are consistent with the NEI model. It should be noted that in the NEI model, the time delays of dipolarization at various magnetotail locations are not related by propagation speed of any wave. As explained in section 3.5 of *Lui et al.* [2007], the spreading of current disruption involves the sum of the time scales in plasma sheet thinning of the next current disruption site and in the nonlinear growth of the excited waves for dipolarization. The time scale for plasma sheet thinning has to be long enough such that the local current density can reach the threshold for instability excitation.

5.5. Bursty Bulk Flows

[54] In the evaluation on the observational evidence of magnetic flux pileup from BBFs as the cause of dipolarization, it is relevant to mention that BBFs have a visible auroral signature identified as the north-south auroral streamer originating near the poleward boundary of the auroral oval [e.g., *Henderson et al.*, 1998; *Newell*, 2000]. Therefore, the MTI model would predict such an auroral feature arriving at the initial brightening arc from the poleward direction at substorm onset. This expected optical auroral feature is seldom, if ever, seen. In other words, there is no evidence from the auroral perspective that BBFs cause dipolarization at substorm onset as proposed by the MTI model. *Donovan et al.* [2008] also pointed out this discrepancy with the MTI model with their observations.

[55] Another point related to BBFs is that high-speed plasma flows can be generated by current disruption. *Lui et al.* [1993] have shown that current disruption can cause a strong net force acting on the plasma. A typical value for the net force is 12% of its preactivity $j \times B$ force. For example, if $j = 50 \text{ nA/m}^2$ (*Lui* [2002] showed that j ranges from 27 to 80 nA/m^2 before current disruption onset) and $B = 5 \text{ nT}$ for a plasma with a density of 0.3 cm^{-3} at the preactivity level,

the plasma would be accelerated to ~ 900 km/s in 15 s. Therefore, BBFs are not necessarily due to magnetic reconnection alone.

5.6. Some Relevant Previous Findings

[56] The present result is consistent with the result from a THEMIS-like conjunction of several satellites (LANL, GOES, Polar, Geotail, and Cluster) distributed from the geostationary altitude to $X_{\text{GSM}} \approx -16 R_E$ [Lui et al., 2007] and from an unprecedented conjunction of eleven satellites in the near-Earth magnetotail ($X > -10 R_E$) [Lui et al., 2008]. This scenario fits well with detailed plasma diagnostic of the dipolarization onset mechanism revealed by one event from Wind observations [Chen et al., 2003] and six events (chosen as the best events near the neutral sheet before dipolarization onsets) from Geotail observations [Saito et al., 2008]. Nevertheless, the general applicability of the NEI model to most substorms requires further investigation.

5.7. An Important Lesson Learned

[57] There is another lesson that may be learned from this study relevant to resolving the two paradigms on the substorm onset location in the magnetotail. If the third auroral activation were examined without the consideration of the previous auroral activation, then it may be construed as an individual substorm onset consistent with the midtail initiation scenario. Therefore, it is vital to distinguish between activity from an isolated substorm and activity from continuation of previous activity in order to arrive at a correct interpretation on the time history of substorm development.

[58] **Acknowledgments.** We thank J. P. McFadden, J. W. Bonnell, and H. Singer for availability of THEMIS ESA data, THEMIS EFI data, and GOES magnetometer data, respectively. This work was supported by the NASA contract NAS5-02099 to University of California, Berkeley, by the NSF grant ATM-0630912 and NASA grant NNX07AU74G to The Johns Hopkins University Applied Physics Laboratory, and by the German Ministerium für Wirtschaft und Technologie and the German Zentrum für Luft- und Raumfahrt under grant 50QP0402.

[59] Amitava Bhattacharjee thanks Mostafa El-Alaoui and another reviewer for their assistance in evaluating this paper.

References

- Akasofu, S.-I. (1964), The development of the auroral substorm, *Planet. Space Sci.*, **12**, 273–282, doi:10.1016/0032-0633(64)90151-5.
- Angelopoulos, V. (2008), The THEMIS mission, *Space Sci. Rev.*, doi:10.1007/s11214-008-9336-1, in press.
- Angelopoulos, V., et al. (1992), Bursty bulk flow in the inner central plasma sheet, *J. Geophys. Res.*, **97**, 4027–4039, doi:10.1029/91JA02701.
- Angelopoulos, V., et al. (1994), Statistical characteristics of bursty bulk flow events, *J. Geophys. Res.*, **99**, 21,257–21,280, doi:10.1029/94JA01263.
- Angelopoulos, V., et al. (1997), Magnetotail flow bursts: Association to global magnetospheric circulation, relationship to ionospheric activity and direct evidence for localization, *Geophys. Res. Lett.*, **24**, 2271–2274, doi:10.1029/97GL02355.
- Auster, U., et al. (2008), The THEMIS fluxgate magnetometer, *Space Sci. Rev.*, doi:10.1007/s11214-008-9365-9, in press.
- Bhattacharjee, A., Z. W. Ma, and X. Wang (1998), Dynamics of thin current sheets and their disruption by ballooning instabilities: A mechanism for magnetospheric substorms, *Phys. Plasmas*, **5**, 2001–2009, doi:10.1063/1.872871.
- Bonnell, J. W., et al. (2008), The Electric Field Instrument (EFI) for Themis, *Space Sci. Rev.*, in press.
- Brittnacher, M., K. B. Quest, and H. Karimabadi (1998), A study of the effect of pitch angle and spatial diffusion on tearing instability using a new finite element based linear code, *J. Geophys. Res.*, **103**, 4587–4596, doi:10.1029/97JA03365.
- Chen, L.-J., et al. (2003), Wind observations pertaining to current disruption and ballooning instability during substorms, *Geophys. Res. Lett.*, **30**(6), 1335, doi:10.1029/2002GL016317.
- Cheng, C. Z., and A. T. Y. Lui (1998), Kinetic ballooning instability for substorm onset and current disruption observed by AMPTE/CCE, *Geophys. Res. Lett.*, **25**, 4091–4094, doi:10.1029/1998GL900093.
- Consolini, G., et al. (2005), On the magnetic field fluctuations during magnetospheric tail current disruption: A statistical approach, *J. Geophys. Res.*, **110**, A07202, doi:10.1029/2004JA010947.
- Coppi, B., G. Laval, and R. Pellat (1966), Dynamics of the geomagnetic tail, *Phys. Rev. Lett.*, **16**, 1207–1210, doi:10.1103/PhysRevLett.16.1207.
- Cully, C. M., et al. (2008), The THEMIS digital fields board, *Space Sci. Rev.*, in press.
- Dobias, P., I. O. Voronkov, and J. C. Samson (2004), On linear plasma instabilities during the substorm expansive phase onset, *Phys. Plasmas*, **11**, 2046–2053, doi:10.1063/1.1695357.
- Donovan, E., et al. (2008), Simultaneous THEMIS in situ and auroral observations of a small substorm, *Geophys. Res. Lett.*, **35**, L17S18, doi:10.1029/2008GL033794.
- El-Alaoui, M. (2001), Current disruption during November 24, 1996, substorm, *J. Geophys. Res.*, **106**, 6229–6245, doi:10.1029/1999JA000260.
- Elphinstone, R. D., J. S. Murphree, and L. L. Cogger (1996), What is a global auroral substorm?, *Rev. Geophys.*, **34**, 169–232, doi:10.1029/96RG00483.
- Erickson, G. M. (1995), Substorm theories: United they stand, divided they fall, *Rev. Geophys.*, **33**, 685–692, doi:10.1029/95RG00398.
- Erickson, G. M., et al. (2000), Electromagnetics of substorm onsets in the near-geosynchronous plasma sheet, *J. Geophys. Res.*, **105**, 25,265–25,290, doi:10.1029/1999JA000424.
- Haerendel, G. (1992), Disruption, ballooning or auroral avalanche, in *Proceedings of the First International Conference on Substorms*, Eur. Space Agency Spec. Publ., ESA SP-335, 417–420.
- Henderson, M. G., G. D. Reeves, and J. S. Murphree (1998), Are north-south aligned auroral structures an ionospheric manifestation of bursty bulk flows?, *Geophys. Res. Lett.*, **25**, 3737–3740, doi:10.1029/98GL02692.
- Hones, E. W., Jr. (1973), Plasma flow in the plasma sheet and its relation to substorms, *Radio Sci.*, **8**, 979–990, doi:10.1029/RS008i011p00979.
- Hones, E. W., Jr. (1979), Transient phenomena in the magnetotail and their relations to substorms, *Space Sci. Rev.*, **23**, 393–410, doi:10.1007/BF00172247.
- Le Contel, O., et al. (2001), Possible control of plasma transport in the near-Earth plasma sheet via current-driven Alfvén waves ($f \approx f_{H+}$), *J. Geophys. Res.*, **106**, 10,817–10,827, doi:10.1029/2001JA900013.
- Le Contel, O., et al. (2008), First results of the THEMIS search coil magnetometers, *Space Sci. Rev.*, doi:10.1007/s11214-008-9371-y, in press.
- Lee, L. C., et al. (1998), Entropy antidiffusion instability and formation of a thin current sheet during geomagnetic substorms, *J. Geophys. Res.*, **103**, 29,419–29,428, doi:10.1029/97JA02141.
- Liang, J., et al. (2008), Intensification of preexisting auroral arc at substorm expansion phase onset: Wave-like disruption during the first tens of seconds, *Geophys. Res. Lett.*, **35**, L17S19, doi:10.1029/2008GL033666.
- Liu, W. W. (1997), Physics of the explosive growth phase: Ballooning instability revisited, *J. Geophys. Res.*, **102**, 4927–4931, doi:10.1029/96JA03561.
- Lui, A. T. Y. (1991), A synthesis of magnetospheric substorm models, *J. Geophys. Res.*, **96**, 1849–1856, doi:10.1029/90JA02430.
- Lui, A. T. Y. (1996), Current disruption in the Earth's magnetosphere: Observations and models, *J. Geophys. Res.*, **101**, 13,067–13,088, doi:10.1029/96JA00079.
- Lui, A. T. Y. (2002), Multiscale phenomena in the near-Earth magnetosphere, *J. Atmos. Sol. Terr. Phys.*, **64**, 125–143, doi:10.1016/S1364-6826(01)00079-7.
- Lui, A. T. Y., C.-I. Meng, and S.-I. Akasofu (1976), Search for the magnetic neutral line in the near-Earth plasma sheet: I. Critical reexamination of earlier studies of magnetic field observations, *J. Geophys. Res.*, **81**, 5934–5940, doi:10.1029/JA081i034p05934.
- Lui, A. T. Y., C.-I. Meng, and S.-I. Akasofu (1977a), Search for the magnetic neutral line in the near-earth plasma sheet: 2. Systematic study of IMP 6 magnetic field observation, *J. Geophys. Res.*, **82**, 1547–1565, doi:10.1029/JA082i010p01547.
- Lui, A. T. Y., et al. (1977b), Systematic study of plasma flow during plasma sheet thinnings, *J. Geophys. Res.*, **82**, 4815–4825, doi:10.1029/JA082i029p04815.
- Lui, A. T. Y., et al. (1991), A cross-field current instability for substorm expansions, *J. Geophys. Res.*, **96**, 11,389–11,401, doi:10.1029/91JA00892.
- Lui, A. T. Y., P. H. Yoon, and C.-L. Chang (1993), Quasi-linear analysis of ion Weibel instability in the Earth's neutral sheet, *J. Geophys. Res.*, **98**, 153–163, doi:10.1029/92JA02034.
- Lui, A. T. Y., et al. (2007), Prelude to THEMIS tail conjunction study, *Ann. Geophys.*, **25**, 1001–1009.

- Lui, A. T. Y., et al. (2008), Near-Earth substorm features from multiple satellite observations, *J. Geophys. Res.*, **113**, A07S26, doi:10.1029/2007JA012738.
- Lyon, J. G., et al. (1998), Simulation of the March 9, 1995, substorm: Auroral brightening and the onset of lobe reconnection, *Geophys. Res. Lett.*, **25**, 3039–3042, doi:10.1029/98GL00662.
- Lyons, L. R. (1996), Substorms: Fundamental observational features, distinction from other disturbances, and external triggering, *J. Geophys. Res.*, **101**, 13,011–13,026, doi:10.1029/95JA01987.
- Lyons, L. R., et al. (2002), Relation of substorm breakup arc to other growth-phase auroral arcs, *J. Geophys. Res.*, **107**(A11), 1390, doi:10.1029/2002JA009317.
- Lyons, L. R., et al. (2003), Observations of dayside convection reduction leading to substorm onset, *J. Geophys. Res.*, **108**(A3), 1119, doi:10.1029/2002JA009670.
- McFadden, J. P., et al. (2008), The THEMIS ESA plasma instrument and in-flight calibration, *Space Sci. Rev.*, in press.
- Mende, S. B., et al. (2008), The THEMIS array of ground-based observatories for the study of auroral substorms, *Space Sci. Rev.*, doi:10.1007/s11214-008-9380-x, in press.
- Nagai, T., et al. (1998), Structure and dynamics of magnetic reconnection for substorm onsets with Geotail observations, *J. Geophys. Res.*, **103**, 4419–4440, doi:10.1029/97JA02190.
- Newell, P. T. (2000), An auroral signature decoded, *Nature*, **408**, 42–43, doi:10.1038/35040680.
- Nishida, A., and N. Nagayama (1973), Synoptic survey for the neutral line in the magnetotail during the substorm expansion phase, *J. Geophys. Res.*, **78**, 3782, doi:10.1029/JA078i019p03782.
- Ohtani, S., R. Yamaguchi, M. Nosé, H. Kawano, M. Engebretson, and K. Yumoto (2002), Quiet-time magnetotail dynamics and their implications for the substorm trigger, *J. Geophys. Res.*, **107**(A2), 1030, doi:10.1029/2001JA000116.
- Ohtani, S., H. J. Singer, and T. Mukai (2006), Effects of the fast plasma sheet flow on the geosynchronous magnetic configuration: Geotail and GOES coordinated study, *J. Geophys. Res.*, **111**, A01204, doi:10.1029/2005JA011383.
- Pellat, R., F. V. Coroniti, and P. L. Pritchett (1991), Does ion tearing exist?, *Geophys. Res. Lett.*, **18**, 143–146, doi:10.1029/91GL00123.
- Perraut, S., et al. (2000), Current-driven electromagnetic ion cyclotron instability at substorm onset, *J. Geophys. Res.*, **105**, 21,097–21,107, doi:10.1029/2000JA900059.
- Perraut, S., et al. (2003), Substorm expansion phase: Observations from Geotail, Polar and IMAGE network, *J. Geophys. Res.*, **108**(A4), 1159, doi:10.1029/2002JA009376.
- Pu, Z. Y., et al. (1999), Drift ballooning instability in the presence of a plasma flow: A synthesis of tail reconnection and current disruption for the initiation of substorms, *J. Geophys. Res.*, **104**, 10,235–10,248, doi:10.1029/1998JA900104.
- Raeder, J., et al. (2001), Global simulation of the Geospace Environment Modeling substorm challenge event, *J. Geophys. Res.*, **106**, 381–395, doi:10.1029/2000JA000605.
- Roux, A., et al. (1991), Plasma sheet instability related to the westward traveling surge, *J. Geophys. Res.*, **96**, 17,697–17,714, doi:10.1029/91JA01106.
- Roux, A., et al. (2008), The search coil magnetometer for THEMIS, *Space Sci. Rev.*, in press.
- Saito, M. H., et al. (2008), Ballooning mode waves prior to substorm-associated dipolarizations: Geotail observations, *Geophys. Res. Lett.*, **35**, L07103, doi:10.1029/2008GL033269.
- Sarafopoulos, D. V. (2008), A physical mechanism producing suprathermal populations and initiating substorms in the Earth's magnetotail, *Ann. Geophys.*, **26**, 1617–1639.
- Schindler, K. (1974), A theory of the substorm mechanism, *J. Geophys. Res.*, **79**, 2803–2810, doi:10.1029/JA079i019p02803.
- Shiokawa, K., W. Baumjohann, and G. Haerendel (1997), Braking of high-speed flows in the near-Earth tail, *Geophys. Res. Lett.*, **24**, 1179–1182, doi:10.1029/97GL01062.
- Shiokawa, K., G. Haerendel, and W. Baumjohann (1998), Azimuthal pressure gradient as driving force of substorm currents, *Geophys. Res. Lett.*, **25**, 959–962, doi:10.1029/98GL00540.
- Shue, J.-H., et al. (2008), Two classes of earthward fast flows in the plasma sheet, *J. Geophys. Res.*, **113**, A02205, doi:10.1029/2007JA012456.
- Sitnov, M. I., H. V. Malova, and A. T. Y. Lui (1997), Quasineutral sheet filamentation instability induced by electron preferential acceleration from stochasticity, *J. Geophys. Res.*, **102**, 163–173, doi:10.1029/96JA01872.
- Spanwick, E., et al. (2007), Ground based identification of dispersionless electron injections, *Geophys. Res. Lett.*, **34**, L03101, doi:10.1029/2006GL028329.
- Tanaka, T. (2000), The state transition model of the substorm onset, *J. Geophys. Res.*, **105**, 21,081–21,096, doi:10.1029/2000JA900061.
- Voronkov, I., et al. (1997), Coupling of shear flow and pressure gradient instabilities, *J. Geophys. Res.*, **102**, 9639–9650, doi:10.1029/97JA00386.
- Zelenyi, L., et al. (2008), Marginal stability of thin current sheets in the Earth's magnetotail, *J. Atmos. Sol. Terr. Phys.*, **70**, 325–333, doi:10.1016/j.jastp.2007.08.019.
- V. Angelopoulos, Institute of Geophysics and Planetary Physics, University of California, 6863 Slichter Hall, Los Angeles, CA 90095, USA.
- H. U. Auster, Institut für Geophysik und Extraterrestrische Physik, Technische Universität Braunschweig, D-38106 Braunschweig, Germany.
- E. Donovan, Department of Physics and Astronomy, University of Calgary, Calgary, AB T2N 1N4, Canada.
- M. O. Fillingim, H. Frey, and D. Larson, Space Sciences Laboratory, University of California, Berkeley, CA 94720, USA.
- O. LeContel, Centre d'Etude des Environnements Terrestre et Planétaires, Institut Pierre-Simon Laplace, 10-12 Avenue de l'Europe, F-78140 Vélizy, France.
- X. Li and W. Liu, Laboratory for Atmospheric and Space Physics, University of Colorado, Boulder, CO 80303, USA.
- A. T. Y. Lui, Applied Physics Laboratory, Johns Hopkins University, 11100 Johns Hopkins Road, Laurel, MD 20723-6099, USA. (tony.lui@jhuapl.edu)
- M. Nosé, Department of Geophysics, Graduate School of Science, Kyoto University, Kitashirakawa Oiwake-cho, Sakyo-ku, Kyoto 606-8502, Japan.
- D. G. Sibeck, NASA Goddard Space Flight Center, Code 674, Greenbelt, MD 20723, USA.